IEEE Access
Multidisciplinary | Rapid Review | Open Access Journal

Received June 7, 2020, accepted July 10, 2020, date of publication July 14, 2020, date of current version July 24, 2020.

Digital Object Identifier 10.1109/ACCESS.2020.3009204

Analytical Bifurcation Tree of Period-1 to Period-4 Motions in a 3-D Brushless DC Motor With Voltage Disturbance

ZHAOBO CHEN, YEYIN XU, AND JIAYANG YING
Department of Mechatronics Engineering, Harbin Institute of Technology, Harbin 150001, China
Corresponding author: Yeyin Xu (xuyeyin@hotmail.com)

ABSTRACT In this paper, the bifurcation trees of analytical solutions of a 3-D brushless DC motor with the voltage disturbance are obtained through the generalized harmonic balance method. The electrical and mechanical model of the 3-D brushless motor is transformed to the dynamic system of coefficients of finite Fourier series. Stable and unstable analytical solutions of the 3-D brushless motor are solved based on such a Fourier series coefficient system. Bifurcation trees of analytical solutions of period-1 to period-2 and period-1 to period-4 motions are achieved. Stability and bifurcations of the analytical solutions of the 3-D brushless motor are determined by the eigenvalues of Jacobian matrix of the coefficient dynamic system. Frequency-amplitude characteristics of periodic motions are presented for a better understanding of the motion complexity in frequency domain. Numerical illustrations are completed for comparison of the analytical solutions with numerical results. The complex dynamics of the 3-D brushless motor are exhibited through the bifurcation trees of analytical solutions.

INDEX TERMS Brushless DC motor, analytical solutions, stability, bifurcation tree.

I. INTRODUCTION

The brushless DC motor is widely used in engineering. It can produce much higher torque and lower noise than DC brushed motor with the same weight. The elimination of physical contact between the brush and commutator allows the motor run more stable and reliable. However, it's difficult to establish the mathematical model for such brushless DC motor. Without the voltage disturbance, in 1993, Hemati [1] first formulated a compact representation of autonomous third order nonlinear differential equations of a brushless DC motor. With this nonlinear brushless DC motor system, the dynamic characteristics of chaotic motions were discussed. Based on Hemati's model, Ge and Chang [2] studied the periodic and chaotic motions of a brushless DC motor through numerical method. The bifurcation diagrams and Lyapunov exponents were presented in their research. In 1995, Kang and Sul [3] applied torque control method for the investigation of the brushless DC motor. The simulation and experimental results showed the torque control method could attenuate the torque ripple. In 2000, Rubaai *et al.* [4] studied the identification and control of the brushless DC motor through online training of dynamic neural networks. The dynamic system of the stator was transformed to a second-order nonlinear differential equations. Numerical method was applied to investigate the dynamic response of the brushless DC motor system. In 2003, Lee and Ehsani [5] built a new simulation model of the brushless DC rotor based on trapezoidal back waveforms to monitor and predict the steady-state response. In 2004, Jabbar *et al.* [6] applied finite-element method for the investigation of the steady state and dynamic response of the brushless DC motor system. The results from finite-element method were verified by experiment. Luo *et al.* [7], [8] combined the method of dynamic surface control technology, radial basis function neural network and adaptive method for controlling the chaotic motions of the brushless DC motor system. Based on Luo's model, Zhang *et al.* [9] employed the generalized Lyapunov function stability theory and the extremum principle of functions for investigation of the chaotic motions of the brushless DC motor system. The global attractive and positively invariant sets were discussed. In 2012, Jagiea and Gwozdz [10] defined a framework for the comprehensive steady-state time domain analysis of the brushless DC motor. The time-periodic finite

The associate editor coordinating the review of this manuscript and approving it for publication was Hamid Mohammad-Sedighi.

element method was used to study the dynamic response of the brushless DC motor. Based on their solutions, all waveforms in the unique framework can be provided. In 2017, Fasil *et al.* [11] proposed a nonlinear phase variable model to simulate a permanent magnet brushless DC motor. In 2018, Huang and Xiong [12] applied a discrete mapping method to periodically excited brushless DC motor. Analytical expression in terms of finite Fourier series terms is obtained based on semi analytical results.

For the nonlinear system of the brushless DC motor, one uses numerical method for investigation of the steady-state response and chaotic motions. Steady-state responses of nonlinear systems are sensitive to initial conditions when there are coexisting periodic solutions. Numerical method has difficulties to capture these coexisting periodic solutions. Besides, the bifurcation trees from periodic motions into chaos and out of chaos are also difficult to be achieved through numerical method. In 2012, Luo [13], [14] developed a generalized harmonic balance method for the analytical solutions of nonlinear systems. The generalized harmonic balance method transforms the original nonlinear system into the dynamic system of coefficients of finite Fourier series. In 2016, Ying *et al.* [15] obtained symmetric period-1 motion to asymmetric period-2 motion and the independent priod-2 and period-4 motion in a Duffing oscillator through generalized harmonic balance method. In 2017, Xu *et al.* [16] applied the generalized harmonic balance method for the stable and unstable analytical solutions of a first-order nonlinear system with a cubic term. The bifurcation branches of symmetric and asymmetric analytical solutions were obtained and jumping phenomenon was observed.

In this paper, the electrical and mechanical model of the 3-D brushless motor with voltage disturbance will be presented first. Then the nonlinear dynamic system of 3-D brushless is transformed to a dynamic system of coefficients of finite Fourier series through generalized harmonic balance method. Analytical solutions of period-1 to period-2 and period-1 to period-4 motions will be obtained from the coefficient dynamic system. Saddle node and Hopf bifurcations are determined by the eigenvalues of Jacobian matrix. The analytical bifurcation tree from period-1 to chaos will be demonstrated through the analytical route of period-1 to period-4 motions. Numerical results will be performed to verify the analytical solutions.

II. MATHEMATICAL MODEL AND ANALYTICAL SOLUTIONS

Consider a brushless DC motor, the electrical and mechanical dynamic equations can be given as ([9]):

$$\begin{aligned}\frac{\mathrm{d}I_q}{\mathrm{d}t} &= \frac{1}{L_q}\left[-RI_q - n\omega\left(L_dI_d + k_t\right) + u_q\right],\\ \frac{\mathrm{d}I_d}{\mathrm{d}t} &= \frac{1}{L_d}\left[-RI_d + n\omega L_qI_q + u_d\right],\\ \frac{\mathrm{d}\omega}{\mathrm{d}t} &= \frac{n}{J}\left[k_tI_q + \left(L_d - L_q\right)I_qI_d\right] - \frac{1}{J}\left(b\omega + T_L\right), \end{aligned} \quad (1)$$

where I_q and I_d are the quadrature-axis and direct-axis currents; u_q and u_d are the quadrature-axis and direct-axis voltages; n is the number of permanent pole pairs; ω is the angular velocity; R is the winding resistance; L_q and L_d are the quadrature-axis and direct-axis fictitious inductance; k_e and $k_t = \sqrt{1.5}k_e$ the permanent-magnet flux constants; b is the viscous damping coefficient; T_L is the additional torque.

The system in (1) can be transformed to a compact form. Based on the affine and the single time scaling transformations [1], the nondimensionalized system of (1) can be obtained.

Define new variables as

$$i_q = \frac{I_q}{\alpha_1}, \quad i_d = \frac{I_d}{\alpha_2} + \frac{k_t}{L_d\alpha_2} + \rho, \ \omega_\tau = \frac{\omega}{\alpha_3}, \ \tau = \frac{tR}{L_q} \quad (2)$$

where

$$\begin{aligned}\alpha_1 &= \frac{-\delta k_t \pm \sqrt{\delta^2k_t^2 - 4\rho\delta\zeta L_qb\alpha_3^2/R}}{2\rho\delta\zeta},\\ \alpha_2 &= \delta\alpha_1, \quad \alpha_3 = \frac{R}{nL_q}, \ \zeta = L_d - L_q, \ \delta = \frac{L_q}{L_d}. \end{aligned} \quad (3)$$

and

$$\begin{aligned}v_q &= \frac{1}{\alpha_1R}u_q, v_d = \frac{L_q}{\alpha_2RL_d}[u_d + R(\rho\alpha_2 + \frac{k_t}{L_d})],\\ \bar{T}_L &= \frac{L_q}{J\alpha_3R}T_L, \quad \sigma = \frac{L_qb}{JR}, \ \eta = \frac{\zeta\alpha_1\alpha_2}{J\alpha_3^2}. \end{aligned} \quad (4)$$

Substitute (2), (3) and (4) into (1), a nondimensional system of the 3-D brushless motor is obtained as

$$\begin{aligned}\frac{\mathrm{d}i_q}{\mathrm{d}\tau} &= v_q - i_q - i_d\omega_\tau + \rho\omega_\tau,\\ \frac{\mathrm{d}i_d}{\mathrm{d}\tau} &= v_d - \delta i_d + i_q\omega_\tau,\\ \frac{\mathrm{d}\omega_\tau}{\mathrm{d}\tau} &= \sigma(i_q - \omega_\tau) + \eta i_qi_d - \bar{T}_L. \end{aligned} \quad (5)$$

Consider the quadrature-axis voltage disturbance as $v_q + Q_0\cos\Omega t$, equations (5) are rewritten as

$$\dot{\mathbf{I}} = \mathbf{F}(\mathbf{I}, \tau) \quad (6)$$

where

$$\mathbf{I} = (i_1, i_2, i_3)^{\mathrm{T}}, \quad \mathbf{F} = (f_1, f_2, f_3)^{\mathrm{T}} \quad (7)$$

and

$$\begin{aligned}i_1 &= i_q, \quad i_2 = i_d, \ i_3 = \omega_\tau\\ f_1 &= v_q - i_q - i_d\omega_\tau + \rho\omega_\tau + Q_0\cos(\Omega\tau),\\ f_2 &= v_d - \delta i_d + i_q\omega_\tau,\\ f_3 &= \sigma(i_q - \omega_\tau) + \eta i_qi_d - \bar{T}_L. \end{aligned} \quad (8)$$

Note that; Q_0 and Ω are disturbance amplitude and frequency, respectively.

From (2) to (8), the 3-D brushless motor system is transformed to a nondimensional nonlinear motor system. Since the steady state solution of motor system in (6) is a periodic

motion, by generalized harmonic balance method, the analytical solution of order-m of such a nonlinear 3-D brushless motor system can be expressed as finite Fourier series form as

$$i_i^* = a_{0i}^{(m)}(t) + \sum_{k=1}^{N} b_{i,k/m}(t)\cos\frac{k}{m}\Omega t + c_{i,k/m}(t)\sin\frac{k}{m}\Omega t \quad (9)$$

where $a_{0i}^{(m)}(t)$, $b_{i,k/m}(t)$ and $c_{i,k/m}(t)$ $(i = 1, 2, 3)$ are the coefficients varying with time. m is period of the analytical solutions. The derivative of (9) gives

$$\dot{i}_1^* = \dot{a}_{0i}^{(m)} + \sum_{k=1}^{N}(\dot{b}_{i,k/m} + \frac{k}{m}\Omega c_{i,k/m})\cos\frac{k}{m}\Omega t + (\dot{c}_{i,k/m} - \frac{k}{m}\Omega b_{i,k/m})\sin\frac{k}{m}\Omega t \quad (10)$$

Note that $a_{0i}^{(m)} = a_{0i}^{(m)}(t)$, $b_{i,k/m} = b_{i,k/m}(t)$ and $c_{i,k/m} = c_{i,k/m}(t)$.

Substitution of (9) and (10) to (6) gives a nonlinear system of coefficients as

$$\begin{aligned}
\dot{\mathbf{a}}_0^{(m)} &= \mathbf{F}_0^{(m)}(\mathbf{a}_0^{(m)}, \mathbf{b}^{(m)}, \mathbf{c}^{(m)}),\\
\dot{\mathbf{b}}^{(m)} &= -\Omega\frac{\mathbf{k}_1}{m}\mathbf{c}^{(m)} + \mathbf{F}_1^{(m)}(\mathbf{a}_0^{(m)}, \mathbf{b}^{(m)}, \mathbf{c}^{(m)}),\\
\dot{\mathbf{c}}^{(m)} &= \Omega\frac{\mathbf{k}_1}{m}\mathbf{b}^{(m)} + \mathbf{F}_2^{(m)}(\mathbf{a}_0^{(m)}, \mathbf{b}^{(m)}, \mathbf{c}^{(m)}).
\end{aligned} \quad (11)$$

where

$$\begin{aligned}
\mathbf{a}_0^{(m)} &= (a_{01}^{(m)}, a_{02}^{(m)}, a_{03}^{(m)})^{\mathrm{T}}\\
\mathbf{b}^{(m)} &= (\mathbf{b}_{1/m}, \mathbf{b}_{2/m}, \cdots, \mathbf{b}_{N/m})^{\mathrm{T}},\\
\mathbf{b}_{k/m} &= (b_{1,k/m}, b_{2,k/m}, b_{3,k/m})^{\mathrm{T}},\\
\mathbf{c}^{(m)} &= (\mathbf{c}_{1/m}, \mathbf{c}_{2/m}, \cdots, \mathbf{c}_{N/m})^{\mathrm{T}},\\
\mathbf{c}_{k/m} &= (c_{1,k/m}, c_{2,k/m}, c_{3,k/m})^{\mathrm{T}},\\
\mathbf{F}_0^{(m)} &= (F_{01}^{(m)}, F_{02}^{(m)}, F_{03}^{(m)})^{\mathrm{T}},\\
\mathbf{F}_1^{(m)} &= (\mathbf{F}_{11}^{(m)}, \mathbf{F}_{12}^{(m)}, \cdots, \mathbf{F}_{1N}^{(m)})^{\mathrm{T}},\\
\mathbf{F}_{1k}^{(m)} &= (F_{1k,1}^{(m)}, F_{1k,2}^{(m)}, F_{1k,3}^{(m)})^{\mathrm{T}},\\
\mathbf{F}_2^{(m)} &= (\mathbf{F}_{21}^{(m)}, \mathbf{F}_{22}^{(m)}, \cdots, \mathbf{F}_{2N}^{(m)})^{\mathrm{T}},\\
\mathbf{F}_{2k}^{(m)} &= (F_{2k,1}^{(m)}, F_{2k,2}^{(m)}, F_{2k,3}^{(m)})^{\mathrm{T}},\\
\mathbf{k}_1 &= diag\,[\mathbf{I}_{3\times3}, 2\mathbf{I}_{3\times3}, \cdots, N\mathbf{I}_{3\times3}].
\end{aligned} \quad (12)$$

for $N = 1, 2, 3, \cdots, \infty$.
and

$$\begin{aligned}
\mathbf{F}_0^{(m)}(\mathbf{a}_0^{(m)}, \mathbf{b}^{(m)}, \mathbf{c}^{(m)}) &= \frac{1}{mT}\int_0^{mT}\mathbf{F}(\mathbf{I}, \tau)dt,\\
\mathbf{F}_{1k}^{(m)}(\mathbf{a}_0^{(m)}, \mathbf{b}^{(m)}, \mathbf{c}^{(m)}) &= \frac{2}{mT}\int_0^{mT}\mathbf{F}(\mathbf{I}, \tau)\cos(\frac{k}{m}\Omega t)dt,\\
\mathbf{F}_{2k}^{(m)}(\mathbf{a}_0^{(m)}, \mathbf{b}^{(m)}, \mathbf{c}^{(m)}) &= \frac{2}{mT}\int_0^{mT}\mathbf{F}(\mathbf{I}, \tau)\sin(\frac{k}{m}\Omega t)dt,
\end{aligned} \quad (13)$$

for $k = 1, 2, 3, \cdots, N$ with

$$\begin{aligned}
F_{01}^{(m)} &= v_q - a_{01}^{(m)} - a_{02}^{(m)}a_{03}^{(m)} + \rho a_{03}^{(m)} - \sum_{i=1}^{N}\frac{1}{2}(b_{2,i/m}b_{3,i/m} + c_{2,i/m}c_{3,i/m}),\\
F_{02}^{(m)} &= v_d - \delta a_{02}^{(m)} + a_{01}^{(m)}a_{03}^{(m)} + \sum_{i=1}^{N}\frac{1}{2}(b_{1,i/m}b_{3,i/m} + c_{1,i/m}c_{3,i/m}),\\
F_{03}^{(m)} &= \sigma a_{01}^{(m)} - \sigma a_{03}^{(m)} + \eta a_{01}^{(m)}a_{02}^{(m)} - T_L + \eta\sum_{i=1}^{N}\frac{1}{2}(b_{1,i/m}b_{2,i/m} + c_{1,i/m}c_{2,i/m})
\end{aligned} \quad (14a)$$

$$\begin{aligned}
F_{1k,1}^{(m)} &= -b_{1,k/m} - (a_{02}^{(m)}b_{3,k/m} + a_{03}^{(m)}b_{2,k/m}) + \rho b_{k,k/m} + Q_0\delta_m^k - \sum_{i=1}^{N}\sum_{j=1}^{N}\frac{1}{2}(b_{2,i/m}b_{3,j/m}\delta_{2c1} + c_{2,i/m}c_{3,j/m}\delta_{2c2})\\
F_{1k,2}^{(m)} &= -\delta b_{2,k/m} + a_{01}^{(m)}b_{3,k/m} + a_{03}^{(m)}b_{1,k/m} + \sum_{i=1}^{N}\sum_{j=1}^{N}\frac{1}{2}(b_{1,i/m}b_{3,j/m}\delta_{2c1} + c_{1,i/m}c_{3,j/m}\delta_{2c2})\\
F_{1k,3}^{(m)} &= \sigma(b_{1,k/m} - b_{3,k/m}) + \eta(a_{01}^{(m)}b_{2,k/m} + a_{02}^{(m)}b_{1,k/m}) + \eta\sum_{i=1}^{N}\sum_{j=1}^{N}\frac{1}{2}(b_{1,i/m}b_{2,j/m}\delta_{2c1} + c_{1,i/m}c_{1,j/m}\delta_{2c2})
\end{aligned} \quad (14b)$$

$$\begin{aligned}
F_{2k,1}^{(m)} &= -c_{1,k/m} - (a_{02}^{(m)}c_{3,k/m} + a_{03}^{(m)}c_{2,k/m}) + \rho c_{3,k/m} - \sum_{i=1}^{N}\sum_{j=1}^{N}\frac{1}{2}(b_{2,i/m}c_{3,j/m} + b_{3,i/m}c_{2,j/m})\delta_{2s1},\\
F_{2k,2}^{(m)} &= -\delta c_{2,k/m} + (a_{01}^{(m)}c_{3,k/m} + a_{03}^{(m)}c_{1,k/m}) + \sum_{i=1}^{N}\sum_{j=1}^{N}\frac{1}{2}(b_{1,i/m}c_{3,j/m} + b_{3,i/m}c_{1,j/m})\delta_{2s1},\\
F_{2k,3}^{(m)} &= \sigma(c_{1,k/m} - c_{3,k/m}) + \eta(a_{01}^{(m)}c_{2,k/m} + a_{02}^{(m)}c_{1,k/m}) + \eta\sum_{i=1}^{N}\sum_{j=1}^{N}\frac{1}{2}(b_{1,i/m}c_{2,j/m} + b_{2,i/m}c_{1,j/m})\delta_{2s1}
\end{aligned} \quad (14c)$$

The deta functions in (14) are

$$\begin{aligned}
\delta_{301} &= \delta_{i-j+l}^0 + \delta_{i+j-l}^0 + \delta_{i-j-l}^0,\\
\delta_{302} &= \delta_{i-j+l}^0 + \delta_{i+j-l}^0 - \delta_{i-j-l}^0,\\
\delta_{2c1} &= \delta_{i+j}^k + \delta_{|i-j|}^k,\ \delta_{2c2} = -\delta_{i+j}^k + \delta_{|i-j|}^k,\\
\delta_{2s1} &= \delta_{i+j}^k - \mathrm{sgn}(i-j)\delta_{|i-j|}^k,\\
\delta_{3c1} &= \delta_{i+j+l}^k + \delta_{|i+j-l|}^k + \delta_{|i-j+l|}^k + \delta_{|i-j-l|}^k,\\
\delta_{3c2} &= -\delta_{i+j+l}^k + \delta_{|i+j-l|}^k + \delta_{|i-j+l|}^k - \delta_{|i-j-l|}^k,\\
\delta_{3s1} &= -\delta_{i+j+l}^k + \mathrm{sgn}(i+j-l)\delta_{|i+j-l|}^k + \mathrm{sgn}(i-j+l)\delta_{|i-j+l|}^k - \mathrm{sgn}(i-j-l)\delta_{|i-j-l|}^k,
\end{aligned} \quad (15a)$$

$$\delta_{3s2} = \delta^k_{i+j+l} + \mathrm{sgn}(i+j-l)\delta^k_{|i+j-l|} + \mathrm{sgn}(i-j+l)\delta^k_{|i-j+l|} + \mathrm{sgn}(i-j-l)\delta^k_{|i-j-l|}. \tag{15b}$$

and

$$\delta^l_k = \begin{cases} 1 & l = k, \\ 0 & l \neq k. \end{cases} \quad \mathrm{sgn}(k) = \begin{cases} 1 & k \geq 0, \\ -1 & k < 0. \end{cases} \tag{16}$$

Let $\mathbf{z} = (\mathbf{a}_0^{(m)}, \mathbf{b}^{(m)}, \mathbf{c}^{(m)})^{\mathrm{T}}$, equation (11) can be rewritten as

$$\dot{\mathbf{z}}^{(m)} = \mathbf{f}^{(m)}(\mathbf{z}^{(m)}) \tag{17}$$

where

$$\mathbf{f}^{(m)} = (\mathbf{F}_0^{(m)}, -\Omega\frac{\mathbf{k}_1}{m}\mathbf{c}^{(m)} + \mathbf{F}_1^{(m)}, \Omega\frac{\mathbf{k}_1}{m}\mathbf{b}^{(m)} + \mathbf{F}_2^{(m)})^{\mathrm{T}}$$

There are $3(2N+1)$ nonlinear equations in the coefficient system in (17). The periodic solutions of (6) are determined by the constant coefficients of the finite Fourier series in (17). Let $\dot{\mathbf{z}}^{(m)*}$ be the equilibrium of $\mathbf{f}^{(m)}(\mathbf{z}) = \mathbf{0}$, thus

$$\begin{aligned} \mathbf{F}_0^{(m)}(\mathbf{a}_0^{(m)*}, \mathbf{b}^{(m)*}, \mathbf{c}^{(m)*}) &= \mathbf{0}, \\ \mathbf{F}_1^{(m)}(\mathbf{a}_0^{(m)*}, \mathbf{b}^{(m)*}, \mathbf{c}^{(m)*}) &= \mathbf{0}, \\ \mathbf{F}_2^{(m)}(\mathbf{a}_0^{(m)*}, \mathbf{b}^{(m)*}, \mathbf{c}^{(m)*}) &= \mathbf{0}. \end{aligned} \tag{18}$$

By solving the $3(2N+1)$ algebraic equations in (18), the equilibrium point $\mathbf{z}^{(m)*} = (\mathbf{a}_0^{(m)*}, \mathbf{b}^{(m)*}, \mathbf{c}^{(m)*})^{\mathrm{T}}$ can be obtained, and the analytical solutions of the 3-D brushless DC motor system can be achieved. Once the analytical solutions of the brushless motor are achieved, the stability and bifurcations of periodic solutions can be analyzed. In the neighborhood of $\mathbf{z}^{(m)*}$, with $\mathbf{z}^{(m)} = \mathbf{z}^{(m)*} + \Delta\mathbf{z}^{(m)}$, the linearized equations of (17) gives

$$\Delta\dot{\mathbf{z}}^{(m)} = D\mathbf{f}^{(m)}(\mathbf{z}^{(m)*})\Delta\mathbf{z}^{(m)} \tag{19}$$

The Jacobian matrix is obtained as

$$D\mathbf{f}^{(m)}(\mathbf{z}^{(m)*}) = \left.\frac{\partial\mathbf{f}^{(m)}}{\partial\mathbf{z}^{(m)}}\right|_{\mathbf{z}^{(m)*}}, \tag{20}$$

The stability of the 3-D brushless DC motor system is determined by the eigenvalues of the Jacobian matrix.

$$\left|D\mathbf{f}^{(m)}(\mathbf{z}^{(m)*}) - \lambda\mathbf{I}_{3(2N+1)\times 3(2N+1)}\right| = 0 \tag{21}$$

where

$$D\mathbf{f}^{(m)} = \begin{bmatrix} \frac{\partial\mathbf{F}_0^{(m)}}{\partial\mathbf{a}_0^{(m)}} & \frac{\partial\mathbf{F}_0^{(m)}}{\partial\mathbf{b}^{(m)}} & \frac{\partial\mathbf{F}_0^{(m)}}{\partial\mathbf{c}^{(m)}} \\ \frac{\partial\mathbf{F}_1^{(m)}}{\partial\mathbf{a}_0^{(m)}} & \frac{\partial\mathbf{F}_1^{(m)}}{\partial\mathbf{b}^{(m)}} & -\Omega\frac{\mathbf{k}_1}{m} + \frac{\partial\mathbf{F}_1^{(m)}}{\partial\mathbf{c}^{(m)}} \\ \frac{\partial\mathbf{F}_2^{(m)}}{\partial\mathbf{a}_0^{(m)}} & \Omega\frac{\mathbf{k}_1}{m} + \frac{\partial\mathbf{F}_2^{(m)}}{\partial\mathbf{b}^{(m)}} & \frac{\partial\mathbf{F}_2^{(m)}}{\partial\mathbf{c}^{(m)}} \end{bmatrix} \tag{22}$$

From the generalized harmonic balance method, the eigenvalues of $D\mathbf{f}^{(m)}$ are grouped as

$$(n_1, n_2, n_3 | n_4, n_5, n_6) \tag{23}$$

where n_1 is the number of negative real eigenvalues, n_2 is the number of positive real eigenvalues, n_3 is the number of zero eigenvalues, n_4 is the number of the pairs of complex eigenvalues with negative real parts, n_5 is the number of the pairs of complex eigenvalues with positive real parts, n_6 is the number of the pairs of complex eigenvalues with zero real parts.

i. If all the real parts of eigenvalues of $D\mathbf{f}^{(m)}$ are less than zero (i.e. $Re(\lambda_k) < 0, k = 1, 2, \cdots, 3(2N+1)$), the analytical solutions of the 3-D brushless DC motor with truncated harmonic terms are stable.
ii. If at least one real part of eigenvalues of $D\mathbf{f}^{(m)}$ is greater than zero (i.e. $Re(\lambda_k) > 0, k = \{1, 2, \cdots, 3(2N+1)\}$), the analytical solutions of the 3-D brushless DC motor with truncated harmonic terms are unstable.
iii. If the real part of the eigenvalues of $D\mathbf{f}^{(m)}$ equals to zero, bifurcations including Saddle node bifurcation and Hopf bifurcation are determined.

III. FREQUENCY-AMPLITUDE CHARACTERISTICS

The bifurcation trees of analytical solution of period-1 to period-4 motions are presented through frequency-amplitude curves. The harmonic amplitude and phase of the analytical solutions of the 3-D brushless DC motor are.

$$A_{i,k/m} = \sqrt{b^2_{i,k/m} + c^2_{i,k/m}}, \varphi_{i,k/m} = \arctan\frac{c_{i,k/m}}{b_{i,k/m}} \tag{24}$$

Based on (24), the analytical solutions in (9) are modified as

$$i_i^*(t) = a_{0i}^{(m)} + \sum_{k=1}^{N} A_{i,k/m}\cos(\frac{k}{m}\Omega t - \varphi_{i,k/m}), \quad (i = 1, 2, 3) \tag{25}$$

Consider a set of parameters as

$$\begin{aligned} &v_q = 0.168, \quad \rho = 60, \ Q_0 = 10, \ \delta = 0.875, \ v_d = 20.66, \\ &\sigma = 4.15, \quad \eta = 0.26, \ \bar{T}_L = 0.53 \end{aligned} \tag{26}$$

From the chosen parameters, the analytical solutions of period-1 to period-4 motions of the 3D brushless DC motor are obtained. The solid and dashed curves represent stable and unstable analytical solutions, respectively. "SN" and "USN" represent stable and unstable saddle-node bifurcation, respectively. "HB" and "UHB" are for stable and unstable Hopf bifurcation, respectively. P-1, P-2 and P-4 represents period-1, period-2 and period-4 motions, respectively.

In Fig.1, global views of bifurcation trees of analytical solutions of period-1 to period-2 and period-1 to period-4 motions of the 3-D brushless DC motor are presented for $\Omega \in (2.5, 7.5)$. In the interested excitation frequency range, there are two bifurcation trees. The first bifurcation tree is formed by independent analytical solutions of period-1 to

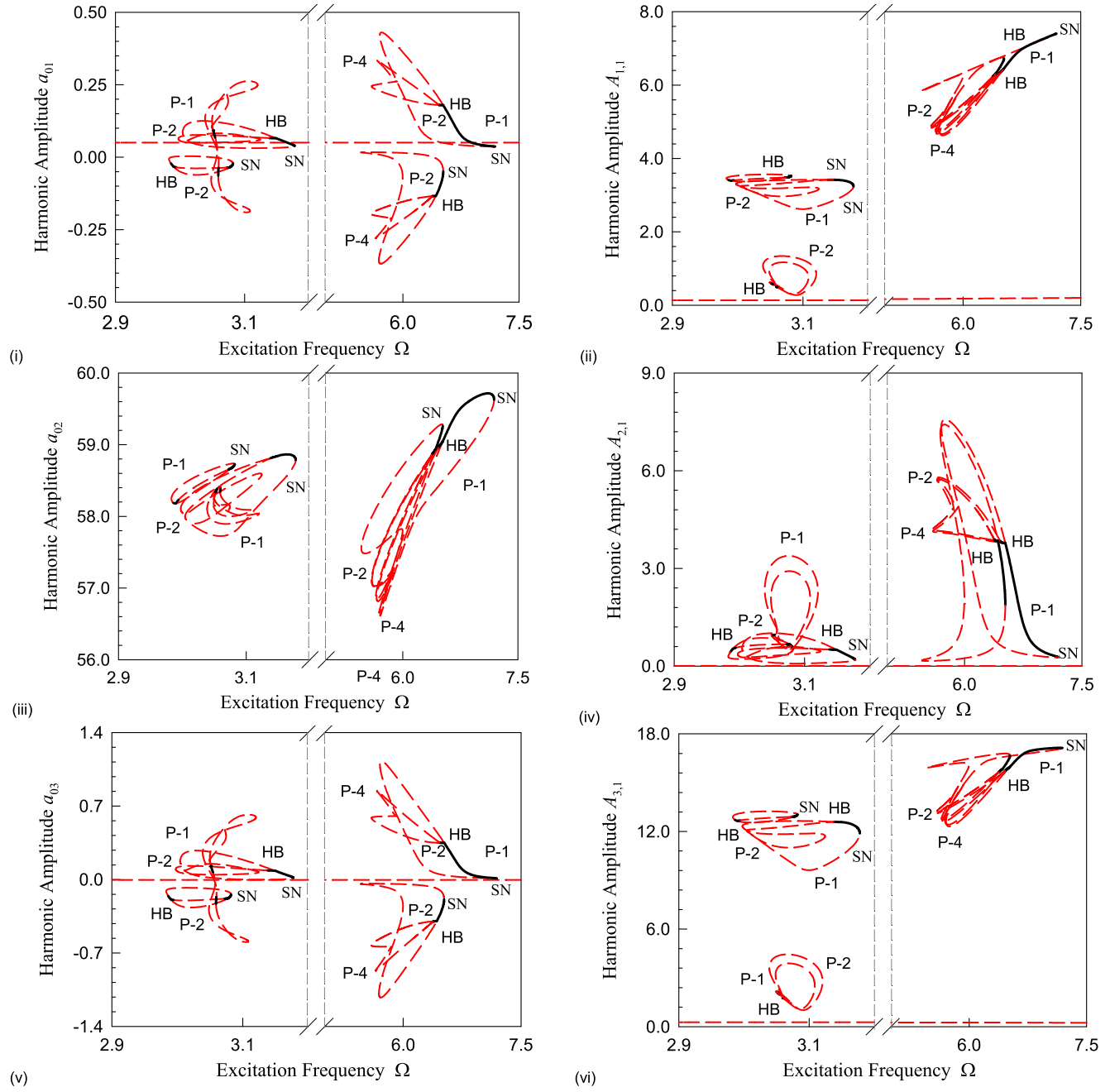

FIGURE 1. A global view of the bifurcation trees of analytical solutions versus with excitation frequency of $\Omega \in (2.5, 7.5)$. (i) constant term a_{01}, (ii) harmonic amplitude $A_{1,1}$, (iii) constant term a_{02}, (iv) harmonic amplitude $A_{2,1}$, (v) constant term a_{03}, (vi) harmonic amplitude $A_{3,1}$.

period-2 in $\Omega \in (2.983, 3.178)$. The second bifurcation tree is formed by independent analytical solutions of period-1 to period-4 in $\Omega \in (5.457, 7.193)$. In Fig.1 (i), the global view of the constant term $a_{01}^{(m)}$ of the analytical solutions of the quadrature-axis i_q current is presented. On left half plane of Fig.1 (i), the analytical solution in terms of $a_{01}^{(m)}$ has three independent bifurcation trees of period-1 to period-2 motions within $\Omega \in (2.983, 3.082), (3.01, 3.118), (3.004, 3.178)$, respectively. On the right half plane of Fig.1 (i), the analytical solution in terms of $a_{01}^{(m)}$ has two independent bifurcation trees of period-1 to period-4 motions within $\Omega \in (5.457, 6.517), (5.698, 7.193)$, respectively. In Fig.1 (ii), the global view of the analytical solution in terms of harmonic amplitude $A_{1,1}$ of the quadrature-axis current i_q is presented. The three independent analytical solutions of period-1 to period-2 are clearly observed. The two analytical solutions of period-1 to period-4 motions overlap with each other. The detail excitation frequency ranges of analytical solutions are presented in Table 1. In Fig.1 (iii), the global view of the analytical solution in terms of $a_{02}^{(m)}$ of the direct-axis current i_d

TABLE 1. Excitation frequency ranges of analytical solution in the 3D brushless DC motor.

No.	Frequency range	Period
1	(2.983, 3.082)	P-1 to P-2
2	(3.010, 3.118)	P-1 to P-2
3	(3.004, 3.178)	P-1 to P-2
4	(5.457, 6.517)	P-1 to P-4
5	(5.698, 7.193)	P-1 to P-4

is presented. Similarly with $a_{01}^{(m)}$, $a_{02}^{(m)}$ only happen in limited frequency range. The quantity level of $a_{02}^{(m)}$ is much bigger than $a_{01}^{(m)}$. The stability frequency ranges and bifurcation points are the same with $a_{01}^{(m)}$. In Fig.1 (iv), the global view of the analytical solutions in terms of harmonic amplitude $A_{2,1}$ of the direct-axis current is presented. On left half plane, three bifurcation trees of the analytical solutions of period-1 to period-2 motions ovelap. On the right half plane, the bifurcation trees of analytical solutions of period-1 to period-4 motions can be clearly observed. $A_{2,1}$ has the same stability and bifurcation points. In Fig,1 (v), the global view of the analytical solution in terms of $a_{03}^{(m)}$ of the angular velocity ω_τ is presented. In Fig.1 (vi), the global view of the analytical solutions in terms of harmonic amplitude $A_{3,1}$ of the angular velocity ω_τ is presented. $a_{03}^{(m)}$ possesses the same curve pattern with $a_{01}^{(m)}$. $A_{3,1}$ possesses the same curve pattern with $A_{1,1}$. $a_{03}^{(m)}$ and $A_{3,1}$ have the same stability frequency range and bifurcation points with $a_{01}^{(m)}$.

In the nonlinear dynamic system of 3-D brushless DC motor shown in (6), the quadrature-axis current i_q, direct-axis current i_d and angular velocity ω_τ have the same stability frequency ranges and bifurcations. To avoid too much illustration, only the bifurcation trees of the analytical solutions of the quadrature-axis current i_q are presented. In Fig.2 (i) and (ii), the zoomed views of the analytical solutions in terms of the constant term $a_{01}^{(m)}$ are presented for $\Omega \in (2.95, 3.22)$ and $(5.00, 7.50)$, respectively. In Fig.2 (i), the three bifurcation trees of the analytical solutions of period-1 to period-2 motions are observed. In the lower bifurcation tree of Fig.2(i), a saddle node bifurcation occurs at $\Omega = 3.082$ which generates jumping. Two Hopf bifurcations occur at $\Omega = 2.986$ and 3.077 where the stable analytical solution of period-1 turns becomes unstable and the analytical solutions of period-2 happens. Another two Hopf bifurcations occur at at $\Omega = 2.993$ and 3.073 where the stable analytical solutions of period-2 becomes unstable. The stable analytical solutions connect with the stable analytical solutions and they form close loops. In the middle bifurcation tree of Fig.2(i), a saddle node bifurcation occurs at $\Omega = 3.177$ and jumping phenomenon happens. A Hopf bifurcation occurs at $\Omega = 3.149$ which turns the stable analytical solution of period-1 to unstable and the analytical solution of period-2 happens. In the cut bifurcation tree, a saddle node bifurcation occurs at $\Omega = 3.591$ which generates jumping. A Hopf bifurcation occurs at $\Omega = 3.598$ which turn the stable analytical solution to be a quasi-periodic solution. At $\Omega = 3.514$, a Hopf bifurcation occurs which generates period-doubling phenomenon that turns the analytical solution of period-1 to period-2. In Fig.2 (ii), the two bifurcation trees of the analytical solutions of period-1 to period-4 are observed. In the lower bifurcation tree, the stable analytical solution becomes unstable after a saddle node bifurcation at $\Omega = 6.522$. Two Hopf bifurcations occur at $\Omega = 6.426$ and $\Omega = 6.385$ which turn the analytical solution of period-1 to period-2 and period-4, respectively. In the upper bifurcation trees, a saddle node bifurcation occurs at $\Omega = 7.194$ and stable analytical solution becomes unstable. Two Hopf bifurcations occur at $\Omega = 6.521$ and 6.473 where the analytical solution of period-1 goes to the analytical solution of period-2 and the analytical solution of period-2 goes to the analytical solution of period-4. In Fig.2 (iii), the analytical solution in terms of the harmonic term $A_{1,1/4}$ is presented. The harmonic term $A_{1,1/4}$ only appear for the analytical solution of period-4. Two Hopf bifurcations occurs at $\Omega = 6.378$ and 6.466 which will turn the analytical solution of period-4 to period-8. In Fig.2 (iv) and (v), the analytical solution in terms of the harmonic term $A_{1,1/2}$ is presented. In Fig.2 (iv), three branches of the analytical solutions of period-2 are clearly observed. $A_{1,1/2}$ is the first harmonic term of the analytical solution of period-2. The stable analytical solutions are connected with the unstable analytical solutions at Hopf bifurcations. In Fig.2 (v), two Hopf bifurcations at $\Omega = 6.385$ and 6.473 turn the analytical solutions of period-2 to period-4. Two unstable Hopf bifurcations at $\Omega = 5.844$ and 5.904 turns the unstable analytical solution of period-4 back to period-2. In Fig.2 (vi), the analytical solution in terms of the harmonic term $A_{1,3/4}$ is presented. $A_{1,3/4}$ has the same stability and bifurcations with $A_{1,1/4}$. In Fig.2 (vii), (viii) and (ix), the zoomed views of the analytical solution of period-1 to period-2 in terms of the harmonic term $A_{1,1}$ are presented. There are two bifurcation trees of the analytical solutions in Fig.2 (vii). The upper bifurcation tree possesses two Hopf bifurcations at $\Omega = 2.986$ and 3.077 which generate the analytical solutions of period-2 from period-1. A saddle node bifurcation at $\Omega = 3.082$ connects the stable and unstable analytical solutions of period-1. The lower bifurcation tree in Fig.2 (vii) possesses one Hopf bifurcation at $\Omega = 3.149$ for period-doubling and a saddle node bifurcation at $\Omega = 3.177$ for connecting the stable and unstable analytical solutions. In Fig.2 (viii), the embedded window clearly shows the bifurcation branches of the analytical solutions. Two Hopf bifurcations at $\Omega = 3.05136$ and 3.05141 are for turning the analytical solutions of period-1 to period-2. One Hopf bifurcation at $\Omega = 3.0544$ is for quasi-periodic analytical solutions. Fig.2 (ix) shows the zoomed view of two bifurcation trees of the analytical solutions of period-1 to period-4. The stability and bifurcations are the same with $a_{01}^{(m)}$ when $\Omega \in (6.3, 6.6)$. In Fig.2 (x), (xi) and (xii), the zoomed views of the analytical solution of period-1 to period-2 in terms of the harmonic term $A_{1,2}$ are presented. $A_{1,2}$ in Fig.2 (x)

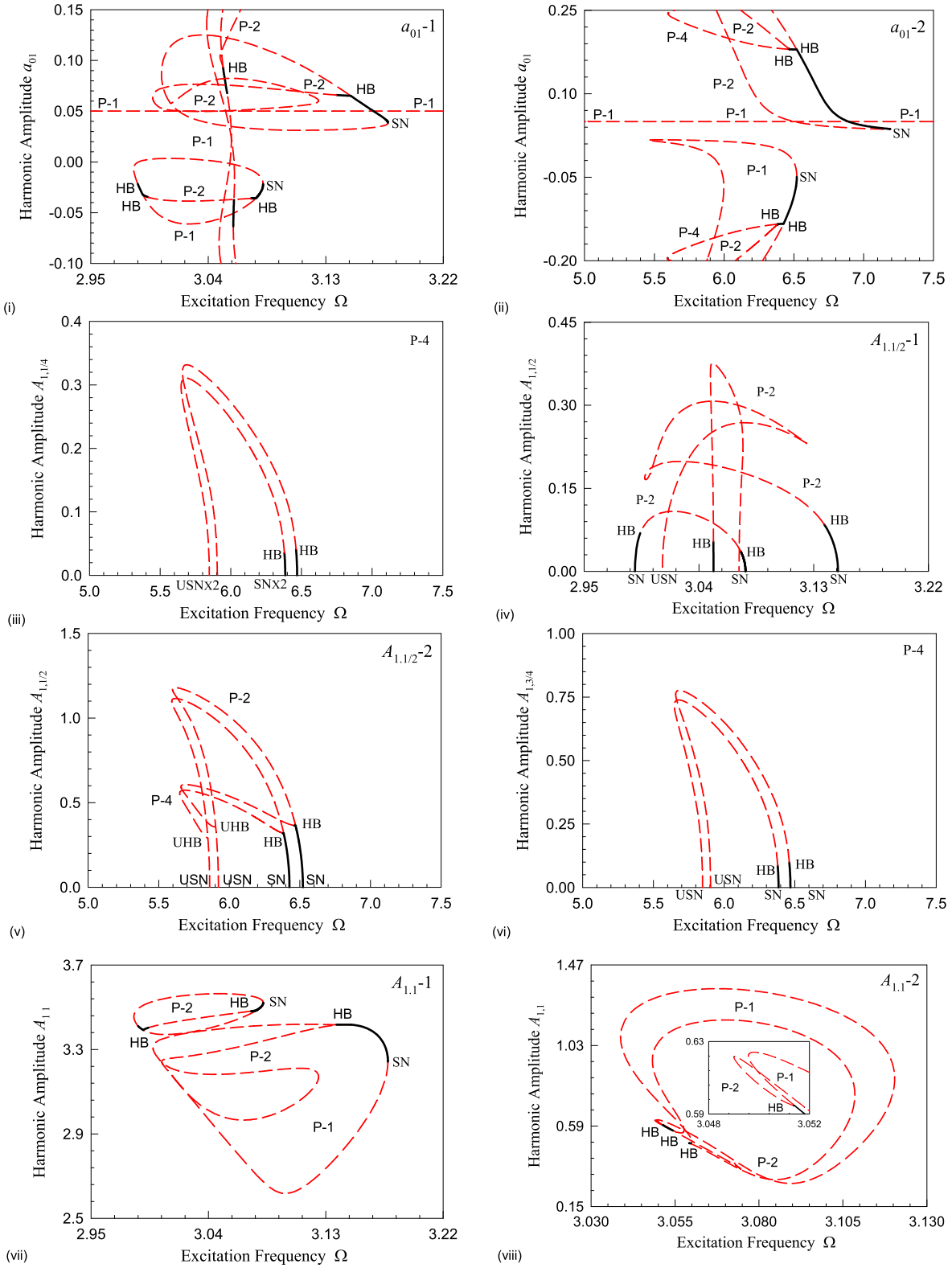

FIGURE 2. The bifurcation trees of analytical solutions versus with excitation frequency of the quadrature-axis current i_q: (i) constant term $a_{01}(1)$; (ii) constant term $a_{01}(2)$; (iii) harmonic amplitude $A_{1,1/4}$; (iv) harmonic amplitude $A_{1,1/2}(1)$; (v) harmonic amplitude $A_{1,1/2}(2)$; (vi) harmonic amplitude $A_{1,3/4}$. (vii) harmonic amplitude $A_{1,1}(1)$; (viii) harmonic amplitude $A_{1,1}(2)$; (ix) harmonic amplitude $A_{1,1}(3)$; (x) harmonic amplitude $A_{1,2}(1)$; (xi) harmonic amplitude $A_{1,2}(2)$; (xii) harmonic amplitude $A_{1,2}(3)$. (xiii) harmonic amplitude $A_{1,3}(1)$; (xiv) harmonic amplitude $A_{1,3}(2)$; (xv) harmonic amplitude $A_{1,3}(3)$; (xvi) harmonic amplitude $A_{1,79/4}(1)$; (xvii) harmonic amplitude $A_{1,20}(1)$; (xviii) harmonic amplitude $A_{1,20}(2)$.

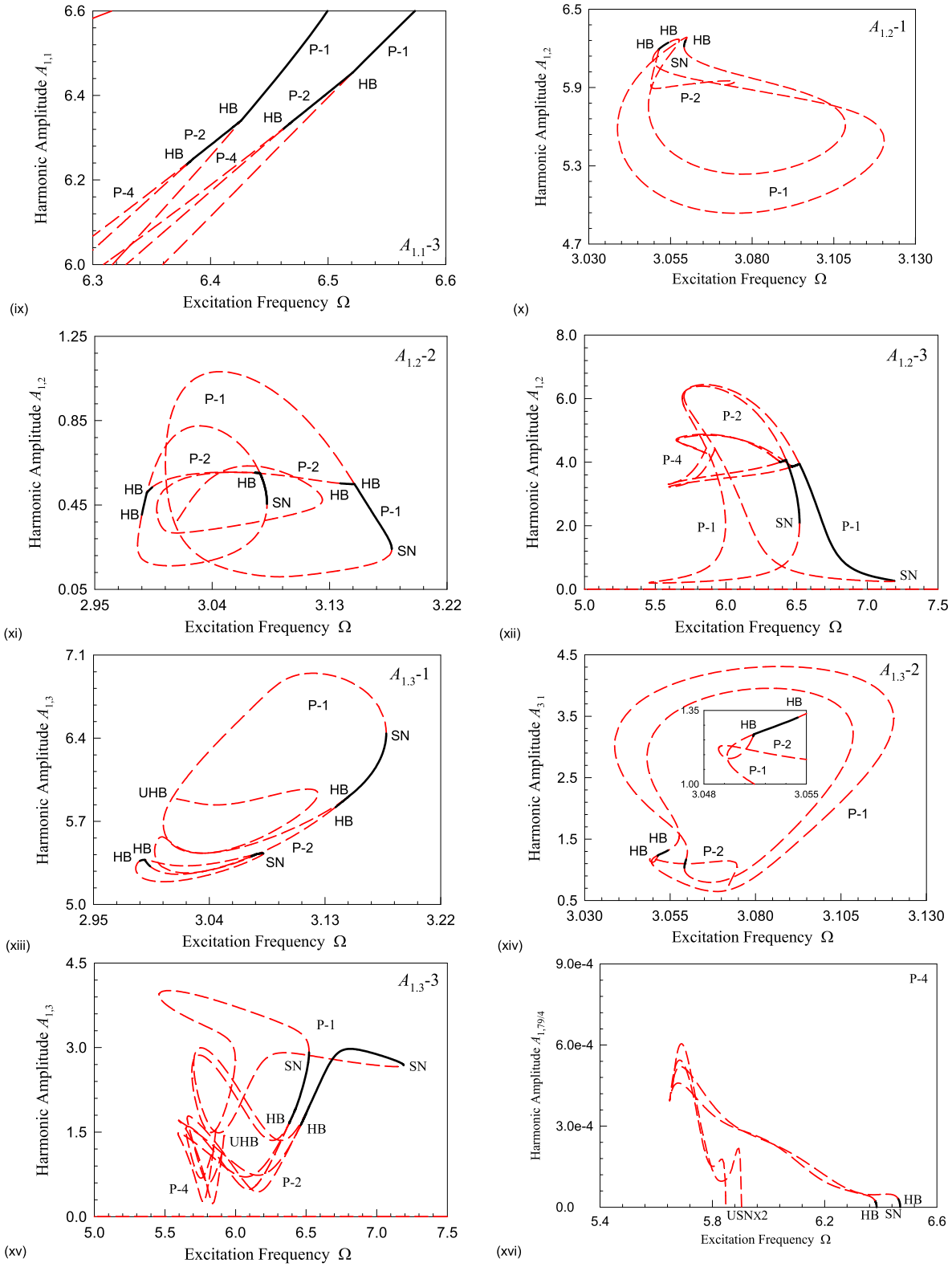

FIGURE 2. *(Continued.)* **The bifurcation trees of analytical solutions versus with excitation frequency of the quadrature-axis current i_q: (i) constant term $a_{01}(1)$; (ii) constant term $a_{01}(2)$; (iii) harmonic amplitude $A_{1,1/4}$; (iv) harmonic amplitude $A_{1,1/2}(1)$; (v) harmonic amplitude $A_{1,1/2}(2)$; (vi) harmonic amplitude $A_{1,3/4}$. (vii) harmonic amplitude $A_{1,1}(1)$; (viii) harmonic amplitude $A_{1,1}(2)$; (ix) harmonic amplitude $A_{1,1}(3)$; (x) harmonic amplitude $A_{1,2}(1)$; (xi) harmonic amplitude $A_{1,2}(2)$; (xii) harmonic amplitude $A_{1,2}(3)$. (xiii) harmonic amplitude $A_{1,3}(1)$; (xiv) harmonic amplitude $A_{1,3}(2)$; (xv) harmonic amplitude $A_{1,3}(3)$; (xvi) harmonic amplitude $A_{1,79/4}(1)$; (xvii) harmonic amplitude $A_{1,20}(1)$; (xviii) harmonic amplitude $A_{1,20}(2)$.**

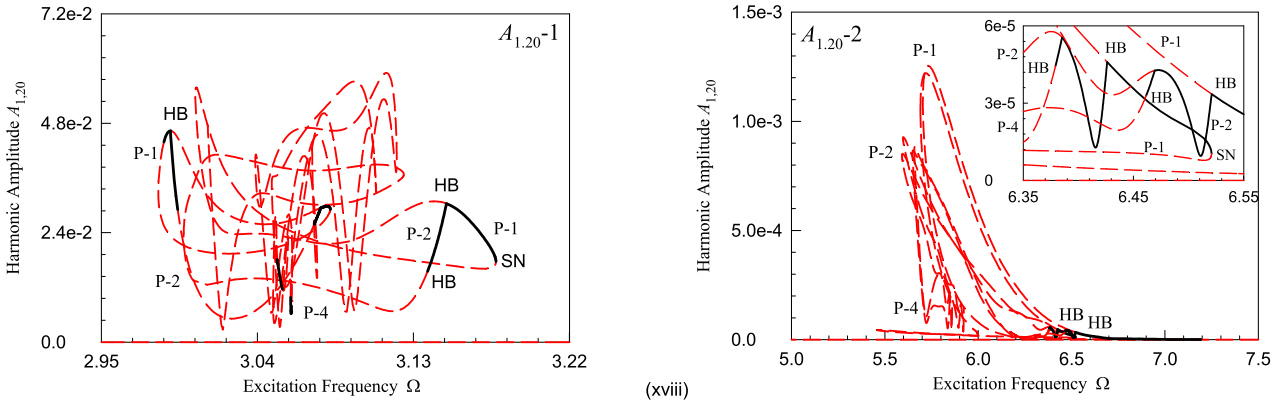

FIGURE 2. *(Continued.)* **The bifurcation trees of analytical solutions versus with excitation frequency of the quadrature-axis current i_q: (i) constant term $a_{01}(1)$; (ii) constant term $a_{01}(2)$; (iii) harmonic amplitude $A_{1,1/4}$; (iv) harmonic amplitude $A_{1,1/2}(1)$; (v) harmonic amplitude $A_{1,1/2}(2)$; (vi) harmonic amplitude $A_{1,3/4}$. (vii) harmonic amplitude $A_{1,1}(1)$; (viii) harmonic amplitude $A_{1,1}(2)$; (ix) harmonic amplitude $A_{1,1}(3)$; (x) harmonic amplitude $A_{1,2}(1)$; (xi) harmonic amplitude $A_{1,2}(2)$; (xii) harmonic amplitude $A_{1,2}(3)$. (xiii) harmonic amplitude $A_{1,3}(1)$; (xiv) harmonic amplitude $A_{1,3}(2)$; (xv) harmonic amplitude $A_{1,3}(3)$; (xvi) harmonic amplitude $A_{1,79/4}(1)$; (xvii) harmonic amplitude $A_{1,20}(1)$; (xviii) harmonic amplitude $A_{1,20}(2)$.**

possesses the same stability and bifurcations with $A_{1,1}$ in Fig.2 (viii). $A_{1,2}$ in Fig.2 (xi) possesses the same stability and bifurcations with $A_{1,1}$ Fig.2 (vii). $A_{1,2}$ in Fig.2 (xii) possesses the same stability and bifurcation with $a_{01}^{(m)}$ Fig.2 (ii). In Fig.2 (xiii), (xiv) and (xv), the zoomed views of the analytical solution of period-1 to period-2 in terms of the harmonic term $A_{1,3}$ are presented. $A_{1,3}$ in Fig.2 (xiii) possesses the same stability and bifurcation with $A_{1,1}$ Fig.2 (viii). $A_{1,3}$ in Fig.2 (xiv) possesses the same stability and bifurcation with $A_{1,1}$ Fig.2 (vii). $A_{1,3}$ in Fig.2 (xv) possesses the same stability and bifurcation with $a_{01}^{(m)}$ Fig.2 (ii). To avoid over illustration, the analytical solution in terms of the harmonic term $A_{1,79/4}$ is presented. $A_{1,79/4}$ has two Hopf bifurcations at $\Omega = 6.378$ and 6.466 and has the quantity level of 1×10^{-4}. In Fig.2 (xvii) and (xviii), the zoomed views of the analytical solution in terms of the harmonic term $A_{1,20}$ are presented. In Fig.2 (xvii), the three bifurcation trees of the analytical solutions of period-1 to period-2 become more complicated. $A_{1,20}$ has the quantity level of 1×10^{-2}. In Fig.2 (xviii), the saddle node and Hopf bifurcation points are clearly shown in the embedded window. $A_{1,20}$ possesses the same stability and bifurcation points as $A_{1,1}$ within the same corresponding frequency range. From the above discussion, at least 40 harmonic terms are needed for the analytical solution of period-1 to period-2 to reach the accuracy of 1×10^{-2} within $\Omega \in (2.95, 3.22)$, and at least 80 harmonic terms are needed for the analytical solution of period-1 to period-4 to reach the accuracy of 1×10^{-3} within $\Omega \in (5.0, 7.5)$.

IV. NUMERICAL ILLUSTRATIONS

In this section, the numerical illustration of the analytical solutions in the 3-D brushless DC motor are presented via mid-point integration method for verification the analytical solutions. Numerical illustrations of stable analytical solutions of period-m ($m = 1, 2$ and 4) are completed. The initial conditions for numerical illustration are extracted from the analytical solutions listed in Table 2. In the following figures, the analytical solutions are depicted by circular symbols. Numerical solutions are depicted by solid curves. Initial conditions and starting points of each period are labeled as "I.C." and "mT" ($m = 1$, 2 and 3).

TABLE 2. **Initial conditions and input data for numerical simulations.**

No.	Ω	Initial condition	Stability
1	6.45	(2.947755,66.370974,19.216232)	stable P-1
2	6.40	(1.172633,66.543098,18.612383)	stable P-1
3	6.381	(1.651893,66.351656,19.005615)	stable P-1

A stable analytical solution of period-1 of the 3-D brushless DC motor is illustrated for $\Omega = 6.45$ in Fig.3. The initial conditions for numerical illustration are $\mathbf{I}_0 = (2.947755, 66.370974, 19.216232)^{\mathrm{T}}$. The $i_q - i_d$ plane (i_q, i_d) of the analytical solution of period-1 is presented in Fig.3 (i). For stable solutions, the analytical results have good agreement with the numerical results. The $i_q - \omega_\tau$ plane (i_q, ω_τ) of the analytical solution is presented in Fig.3 (ii). The analytical and numerical solutions match with each other and they form a simple periodic orbit. The $i_d - \omega_\tau$ plane (i_d, ω_τ) of the analytical solution is presented in Fig.3 (iii). With the initial conditions given, these orbits can be reproduced by other numerical methods like ode45. The $i_q - i_d - \omega_\tau$ 3D orbit (i_q, i_d, ω_τ) of the analytical solution is presented in Fig.3 (iv). The agreement of the analytical and numerical solutions can be observed. To avoid too much illustration, only the harmonic amplitudes of the analytical solutions of the quadrature-axis current i_q and direct-axis current i_d are presented in Fig.3 (v). For quadrature-axis current i_q(white), the constant term is $A_{1,0} = -a_{1,0} \approx 0.1202$. The main harmonic amplitudes are $A_{1,1} \approx 6.4202, A_{1,2} \approx 3.7882, A_{1,3} \approx 2.0872, A_{1,4} \approx 1.9394, A_{1,5} \approx 0.4447, A_{1,6} \approx 0.4968, A_{1,7} \approx 0.2193, A_{1,8} \approx 0.0965, A_{1,9} \approx 0.0692, A_{1,10} \approx 0.0253, A_{1,11} \approx 0.0165$. The rest harmonic amplitudes are $A_{1,j} \in (10^{-10}, 10^{-2})$ ($j = 12, 13, \cdots, 40$). For direct-axis i_d (gray),

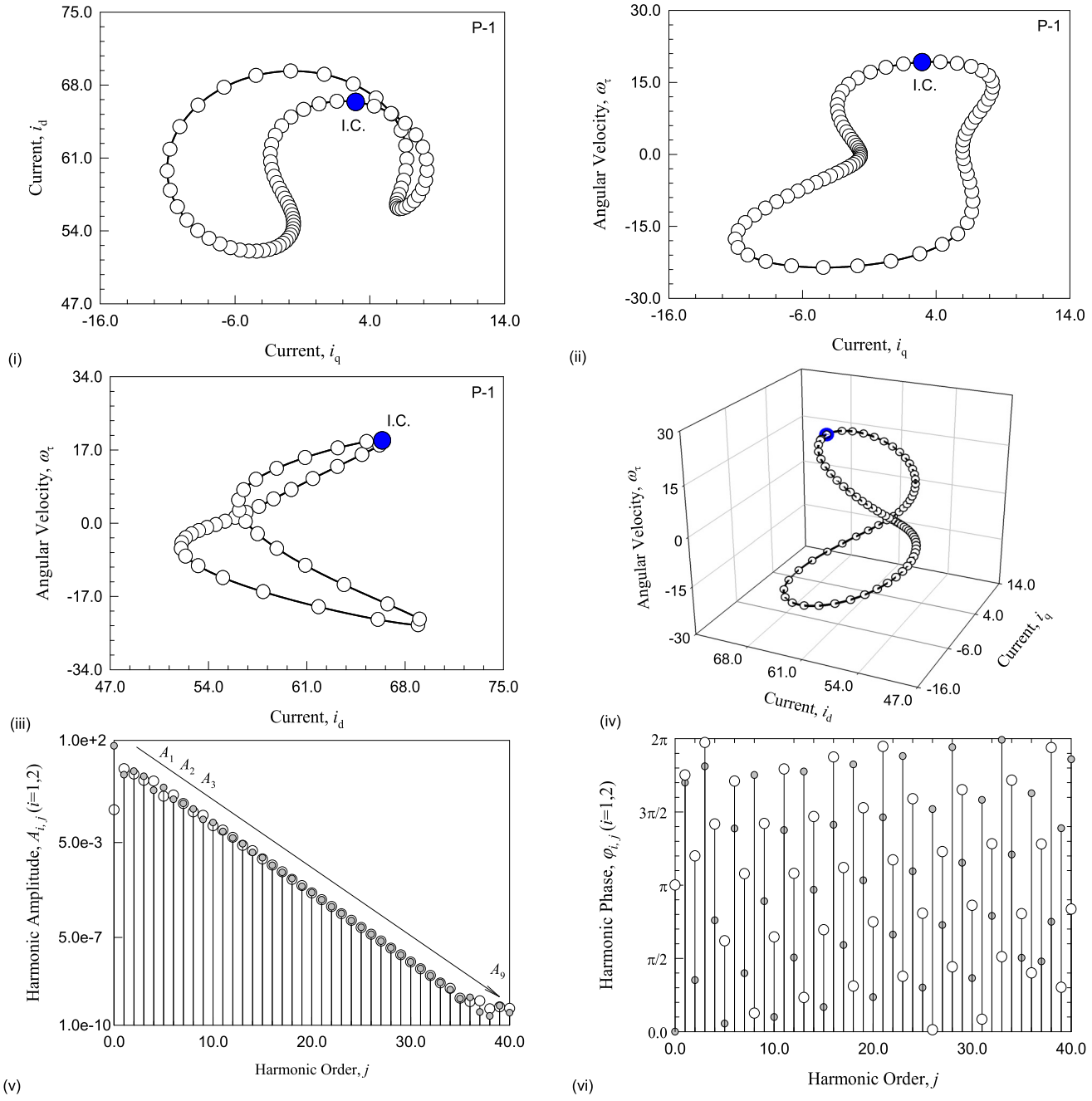

FIGURE 3. A stable analytical solution of period-1 of the 3D brushless motor at $\Omega = 6.45$. (i) $i_q - i_d$ plane (i_q, i_d), (ii) $i_q - \omega_\tau$ plane (i_q, ω_τ), (iii) $i_d - \omega_\tau$ plane (i_d, ω_τ), (iv) $i_q - i_d - \omega_\tau$ curve (i_q, i_d, ω_τ), (v) harmonic amplitude $A_{i,j}$, (vi) harmonic phase $\varphi_{i,j}$ $(i = 1, 2; j = 0, 1, \cdots, 40)$.

$A_{2,0} = a_{2,0} \approx 59.0041, A_{2,1} \approx 3.5550, A_{2,2} \approx 5.0133, A_{2,3} \approx 3.0841, A_{2,4} \approx 0.7933, A_{2,5} \approx 1.0325, A_{2,6} \approx 0.3284, A_{2,7} \approx 0.2201, A_{2,8} \approx 0.1290, A_{2,9} \approx 0.0462, A_{2,10} \approx 0.0346, A_{2,11} \approx 0.0146$ and $A_{2,j} \in (10^{-10}, 10^{-2})$ $(j = 12, 13, \cdots, 40)$. The harmonic phases of the analytical solutions of the quadrature-axis and direct-axis are presented in Fig.6 (vi) with $\varphi_{i,j} \in (0, 2\pi)(i = 1, 2; j = 0, 1, \cdots, 40)$. For such an analytical solution of period-1 with $\Omega = 6.45$, 40 harmonic terms are needed to reach the accuracy of 1×10^{-10}.

A stable analytical solution of period-2 for $\Omega = 6.40$ is illustrated in Fig.4. The initial conditions for numerical illustration are $\mathbf{I}_0^{(2)} = (1.172633, 66.543098, 18.612383)^{\mathrm{T}}$. The $i_q - i_d$, $i_q - \omega_\tau$ and $i_d - \omega_t$ planes $(i_q^{(2)}, i_d^{(2)})$, $(i_q^{(2)}, \omega_\tau^{(2)})$ and $(i_d^{(2)}, \omega_\tau^{(2)})$ are presented in Fig.4 (i), (ii) and (iii). The numerical results match with the analytical results. The period-doubling phenomenon can be clearly observed. The $i_q - i_d$ plane $(i_q^{(2)}, i_d^{(2)})$ has double pattern of (i_q, i_d) shown in Fig.3 (i). The $i_q - \omega_\tau$ plane $(i_q^{(2)}, \omega_\tau^{(2)})$ has double pattern

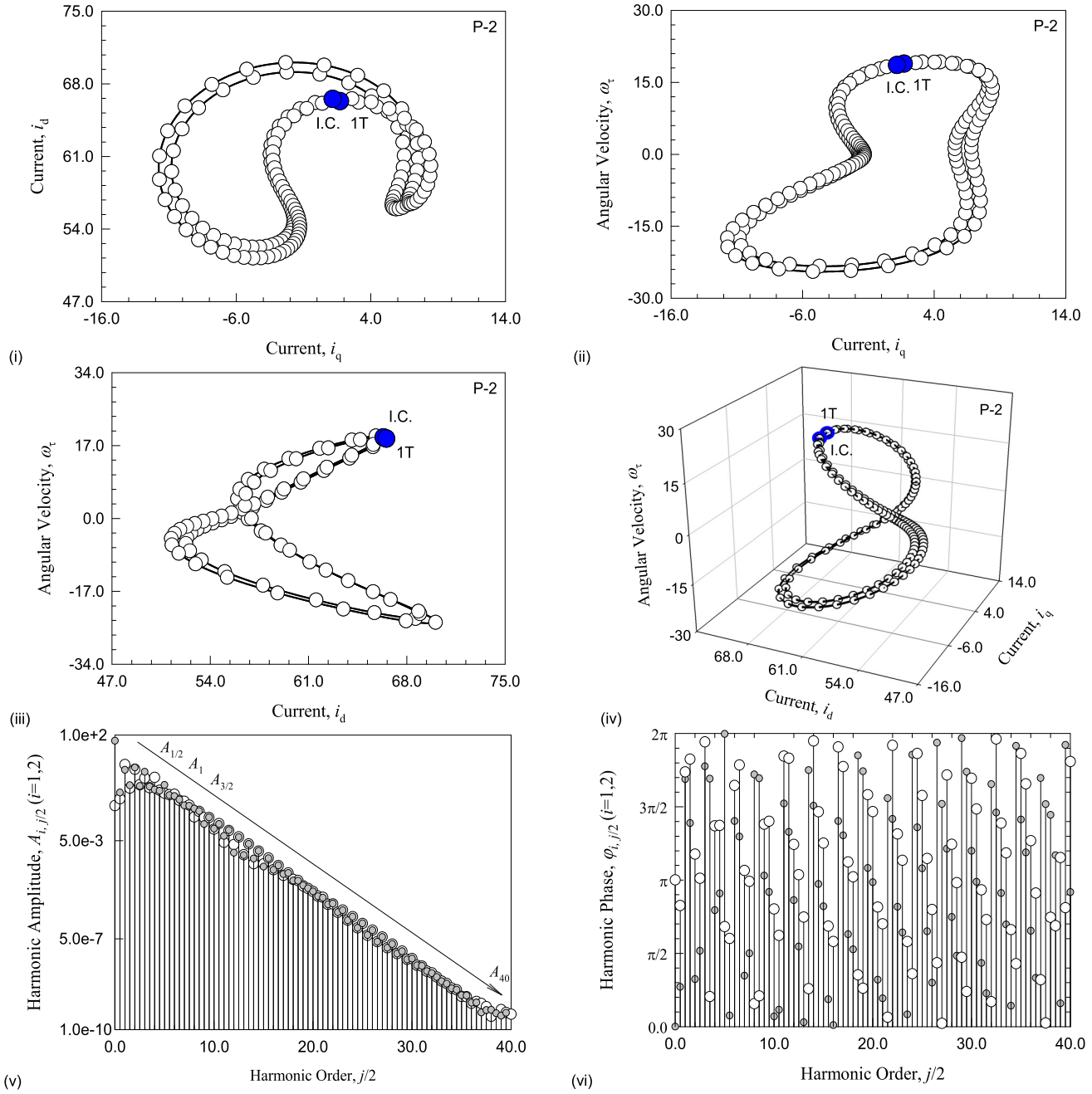

FIGURE 4. A stable analytical solution of period-2 of the 3D brushless motor at $\Omega = 6.40$. (i) $i_q - i_d$ plane $(i_q^{(2)}, i_d^{(2)})$, (ii) $i_q - \omega_\tau$ plane $(i_q^{(2)}, \omega_\tau^{(2)})$, (iii) $i_d - \omega_\tau$ plane $(i_d^{(2)}, \omega_\tau^{(2)})$, (iv) $i_q - i_d - \omega_\tau$ curve $(i_q^{(2)}, i_d^{(2)}, \omega_\tau^{(2)})$, (v) harmonic amplitude $A_{i,j}$, (vi) harmonic phase $\varphi_{i,j}(i = 1, 2; j = 0, 1, \cdots, 40)$.

of (i_q, ω_τ) shown in Fig.3 (ii). The $i_d - \omega_\tau$ plane $(i_d^{(2)}, \omega_\tau^{(2)})$ has double pattern of (i_d, ω_τ) shown in Fig.3 (iii). The 3D orbit $(i_q^{(2)}, i_d^{(2)}, \omega_\tau^{(2)})$ of the analytical solution of period-2 is presented in Fig.4 (iv). The period-doubling phenomenon in Fig.4 (iv) is obvious compared with (i_q, i_d, ω_τ) in Fig.3 (iv). The harmonic amplitudes of quadrature-axis $i_q^{(2)}$ are presented in Fig.4 (v). For $i_q^{(2)}$, the constant term is $A_{1,0/2} = -a_{1,0}^{(2)} \approx 0.1340$. The main harmonic terms are with $A_{1,1/2} \approx 0.2555, A_{1,1} \approx 6.2826, A_{1,3/2} \approx 0.6879, A_{1,2} \approx 4.0259, A_{1,5/2} \approx 0.9492, A_{1,3} \approx 1.7698, A_{1,7/2} \approx 0.7161, A_{1,4} \approx 1.9025$. The rest harmonic terms are $A_{1,j/2} \in (10^{-10}, 10^0)$ $(j = 9, 10, \cdots, 80)$ For i_d, the constant term is $A_{2,0/2} = a_{2,0}^{(2)} \approx 58.8945$. The main harmonic terms are with $A_{2,1/2} \approx 0.4564, A_{2,1} \approx 3.8573, A_{2,3/2} \approx 0.9063, A_{2,2} \approx 4.7583, A_{2,5/2} \approx 0.8444, A_{2,3} \approx 3.1914$. The rest harmonic terms are $A_{2,j/2} \in (10^{-10}, 10^0)$ $(j = 7, 8, \cdots, 80)$. The harmonic phases for $i_q^{(2)}$ and $i_d^{(2)}$ are presented in Fig.4 (vi) with $\varphi_{i,j} \in (0, 2\pi)(i = 1, 2; j = 0, 1, \cdots, 80)$. Such an analytical

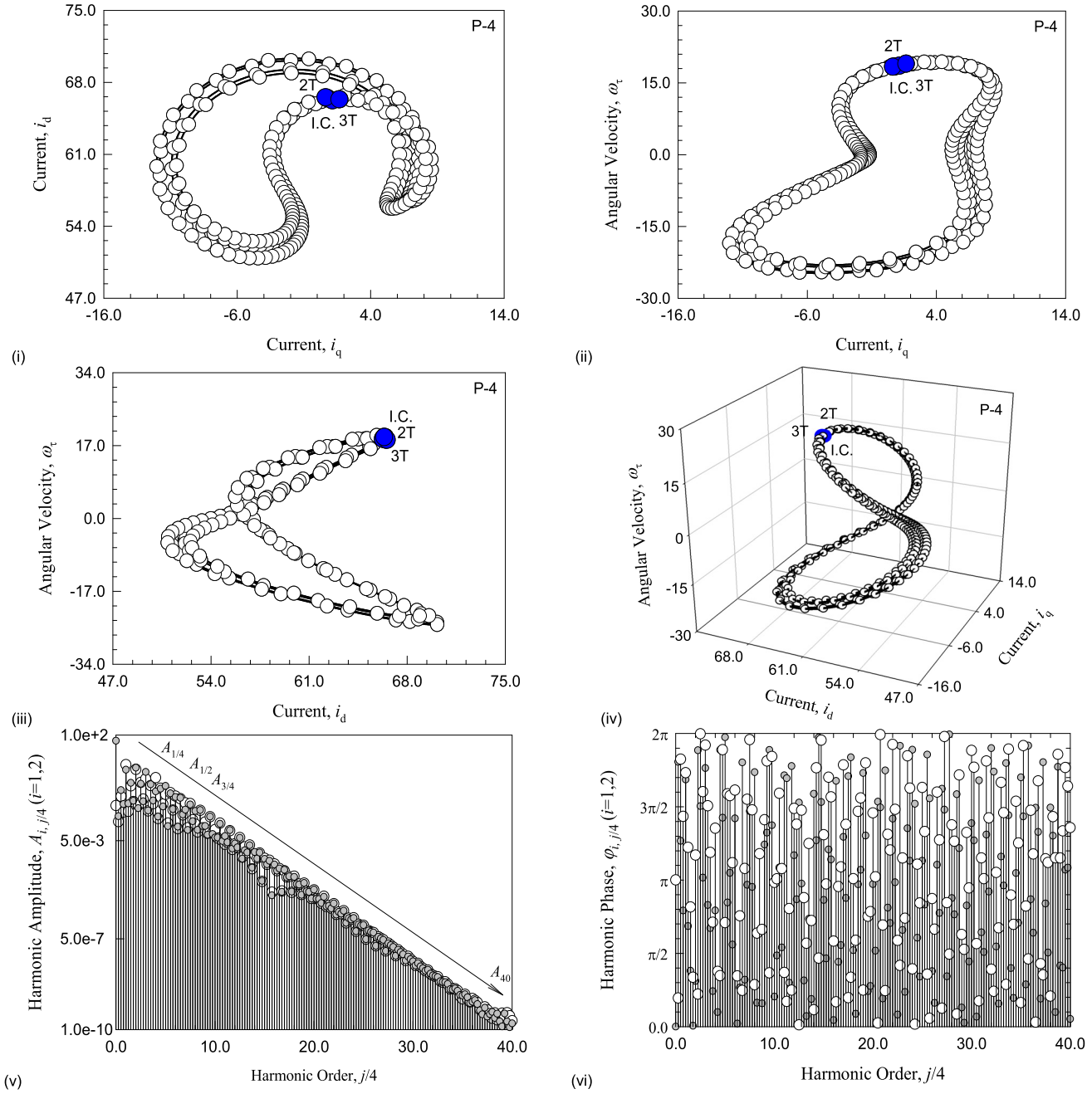

FIGURE 5. A stable analytical solution of period-4 of the 3D brushless motor at $\Omega = 6.381$. (i) $i_q - i_d$ plane $(i_q^{(4)}, i_d^{(4)})$, (ii) $i_q - \omega_\tau$ plane $(i_q^{(4)}, \omega_\tau^{(4)})$, (iii) $i_d - \omega_\tau$ plane $(i_d^{(4)}, \omega_\tau^{(4)})$, (iv) $i_q - i_d - \omega_\tau$ curve $(i_q^{(4)}, i_d^{(4}, \omega_\tau^{(4)})$, (v) harmonic amplitude $A_{i,j}$, (vi) harmonic phase $\varphi_{i,j}$ $(i = 1, 2; j = 0, 1, \cdots, 40)$.

solution of period-2 needs 80 harmonic terms to get appropriate accurate solution of accuracy $\varepsilon < 1 \times 10^{-10}$.

In Fig.5, a stable analytical solution of period-4 is presented for $\Omega = 6.381$. The initial conditions for numerical illustration are $\mathbf{I}_0^{(4)} = (1.651893, 66.351656, 19.005615)^{\mathrm{T}}$. The $i_q - i_d$, $i_q - \omega_\tau$ and $i_d - \omega_t$ planes $(i_q^{(4)}, i_d^{(4)})$, $(i_q^{(4)}, \omega_\tau^{(4)})$ and $(i_d^{(4)}, \omega_\tau^{(4)})$ are presented in Fig.5 (i), (ii) and (iii). The numerical and analytical results match with each other. The $i_q - i_d$ plane $(i_q^{(4)}, i_d^{(4)})$ has double pattern of $(i_q^{(2)}, i_d^{(2)})$ in Fig.4 (i), quadruple pattern of (i_q, i_d) in Fig.3 (i). The $i_q - \omega_\tau$ plane $(i_q^{(4)}, \omega_\tau^{(4)})$ has double pattern of $(i_q^{(2)}, \omega_\tau^{(2)})$ in Fig.4 (ii), and quadruple pattern of (i_q, ω_τ) in Fig.3 (ii). The $i_d - \omega_\tau$ plane $(i_d^{(4)}, \omega_\tau^{(4)})$ has double pattern of $(i_d^{(2)}, \omega_\tau^{(2)})$ in Fig.4 (iii), and quadruple pattern of (i_d, ω_τ) in Fig.3 (iii). The 3D orbit $(i_q^{(4)}, i_d^{(4)}, \omega_\tau^{(4)})$ of the analytical solution of period-4 is presented in Fig.5 (iv). Similarly, $(i_q^{(4)}, i_d^{(4)}, \omega_\tau^{(4)})$ has the double pattern of $(i_q^{(2)}, i_d^{(2)}, \omega_\tau^{(2)})$ in Fig.4 (iv), and quadruple pattern of (i_q, i_d, ω_τ) in Fig. 3 (iv). The period-doubling phenomenon is clearly presented. For such stable analytical solution of period-4, harmonic

amplitudes of $i_q^{(4)}$ and $i_d^{(4)}$ are presented in Fig.5(v). For $i_q^{(4)}$, the constant term is $A_{1,0/4} = -a_{1,0}^{(4)} \approx 0.1352$. The main harmonic terms are $A_{1,1/4} \approx 0.0299, A_{1,1/2} \approx 0.3191, A_{1,3/4} \approx 0.0732, A_{1,1} \approx 6.2395, A_{1,5/4} \approx 0.0775, A_{1,3/2} \approx 0.8515, A_{1,7/4} \approx 0.1950, A_{1,2} \approx 4.0169, A_{1,9/4} \approx 0.1353, A_{1,5/2} \approx 1.1804, A_{1,11/4} \approx 0.2470, A_{1,3} \approx 1.6658, A_{1,13/4} \approx 0.0813, A_{1,7/2} \approx 0.8775, A_{1,15/4} \approx 0.1606$ and $A_{1,4} \approx 1.8312$. The rest harmonic terms are $A_{1,j/4} \in (10^{-10}, 10^{0})$ $(j = 17, 18, \cdots, 160)$. For $i_d^{(4)}$, the constant term is $A_{2,0/4} = a_{2,0}^{(4)} \approx 58.8633$, and the main harmonic terms are $A_{2,1/4} \approx 0.0497, A_{2,1/2} \approx 0.5695, A_{2,3/4} \approx 0.1539, A_{2,1} \approx 3.8807, A_{2,5/4} \approx 0.1633, A_{2,3/2} \approx 1.1340, A_{2,7/4} \approx 0.2124, A_{2,2} \approx 4.6816, A_{2,9/4} \approx 0.1050, A_{2,5/2} \approx 1.0414, A_{2,11/4} \approx 0.2006$ and $A_{2,3} \approx 3.1471$. The rest harmonic terms are $A_{2,j/4} \in (10^{-10}, 10^{0})$ $(j = 13, 14, \cdots, 160)$. The harmonic phases of $i_q^{(4)}$ and $i_d^{(4)}$ are presented in Fig.5 (vi) with $\varphi_{i,j} \in (0, 2\pi)(i = 1, 2; j = 0, 1, \cdots, 160)$. For the accuracy of $\varepsilon = 10^{-10}$, the analytical solution of period-4 needs 160 harmonic terms in the 3-D brushless DC motor system.

V. CONCLUSION

In this paper, the analytical solutions of the 3-D brushless DC motor are obtained through the generalized harmonic balance method. The bifurcation trees of period-1 to period-2 and period-1 to period-4 motions are achieved analytically. The stable and unstable analytical solutions of period-2 motions originated from the stable and unstable Hopf bifurcations of period-1 motions are presented. The stable and unstable analytical solutions of period-4 motions originated from the stable and unstable Hopf bifurcations of period-2 motions are presented. With the analytical solutions, initial conditions for numerical illustrations are obtained and the dynamic characteristics of the 3-D brushless DC motor are investigated. From the analytical solutions, the bifurcation trees revealing the relationship among the independent periodic motions are depicted, which is difficult to be obtained by numerical methods. The close loop curves in harmonic amplitudes formed by stable and unstable analytical solutions are observed. The harmonic results indicate the analytical solutions turn to be more complicated when the disturbance frequency closes to zero. The numerical solutions have good agreement with the analytical solutions. The analytical solutions obtained present new insights of the complex dynamics of the 3-D brushless motor.

REFERENCES

[1] N. Hemati, "Dynamic analysis of brushless motors based on compact representations of the equations of motion," in *Proc. Conf. Rec. IEEE Ind. Appl. Conf. Twenty-Eighth IAS Annu. Meeting*, Toronto, ON, Canada, Oct. 1993, pp. 51–58.

[2] Z.-M. Ge and C.-M. Chang, "Chaos synchronization and parameters identification of single time scale brushless DC motors," *Chaos, Solitons Fractals*, vol. 20, no. 4, pp. 883–903, May 2004.

[3] S.-J. Kang and S.-K. Sul, "Direct torque control of brushless DC motor with nonideal trapezoidal back EMF," *IEEE Trans. Power Electron.*, vol. 10, no. 6, pp. 796–802, Nov. 1995.

[4] A. Rubaai, R. Kotaru, and M. D. Kankam, "A continually online-trained neural network controller for brushless DC motor drives," *IEEE Trans. Ind. Appl.*, vol. 36, no. 2, pp. 475–483, Apr. 2000.

[5] B.-K. Lee and M. Ehsani, "Advanced simulation model for brushless DC motor drives," *Electr. Power Compon. Syst.*, vol. 31, no. 9, pp. 841–868, Sep. 2003.

[6] M. A. Jabbar, H. N. Phyu, Z. Liu, and C. Bi, "Modeling and numerical simulation of a brushless permanent-magnet DC motor in dynamic conditions by time-stepping technique," *IEEE Trans. Ind. Appl.*, vol. 40, no. 3, pp. 763–770, May 2004.

[7] S. Luo, J. Wang, S. Wu, and K. Xiao, "Chaos RBF dynamics surface control of brushless DC motor with time delay based on tangent barrier Lyapunov function," *Nonlinear Dyn.*, vol. 78, no. 2, pp. 1193–1204, Oct. 2014.

[8] S. Luo, S. Wu, and R. Gao, "Chaos control of the brushless direct current motor using adaptive dynamic surface control based on neural network with the minimum weights," *Chaos, Interdiscipl. J. Nonlinear Sci.*, vol. 25, no. 7, Jul. 2015, Art. no. 073102.

[9] F. Zhang, D. Lin, M. Xiao, and H. Li, "Dynamical behaviors of the chaotic brushless DC motors model," *Complexity*, vol. 21, no. 4, pp. 79–85, Mar. 2016.

[10] M. Jagieła and J. Gwoźdź, "Steady-state time-periodic finite element analysis of a brushless DC motor drive considering motion," *Arch. Electr. Eng.*, vol. 64, no. 3, pp. 471–486, Sep. 2015.

[11] M. Fasil, N. Mijatovic, B. B. Jensen, and J. Holboll, "Nonlinear dynamic model of PMBLDC motor considering core losses," *IEEE Trans. Ind. Electron.*, vol. 64, no. 12, pp. 9282–9290, Dec. 2017.

[12] J. Huang and X. Xiong, "Nonlinear behavior for periodically excited brushless motor," *Int. J. Comput. Math. Electr. Electron. Eng.*, vol. 38, no. 2, pp. 522–535, Mar. 2019.

[13] A. C. Luo, *Continuous Dynamical Systems*. Glen Carbon, IL, USA: Higher Education Press, 2012, pp. 109–165.

[14] A. C. Luo, *Analytical Routes to Chaos in Nonlinear Engineering*. Hoboken, NJ, USA: Wiley, 2014.

[15] J. Ying, Y. Jiao, and Z. Chen, "Further analytic solutions for periodic motions in the duffing oscillator," *Int. J. Dyn. Control*, vol. 5, no. 4, pp. 947–964, Dec. 2017.

[16] Y. Xu, A. C. J. Luo, and Z. Chen, "Analytical solutions of periodic motions in 1-dimensional nonlinear systems," *Chaos, Solitons Fractals*, vol. 97, pp. 1–10, Apr. 2017.

ZHAOBO CHEN received the Ph.D. degree in mechanical engineering from the Harbin Institute of Technology, Harbin, China, in 1995. He is currently a Professor with the Harbin Institute of Technology. His current research interests include rotor dynamics, nonlinear dynamics, structure vibration, and acoustic radiation control.

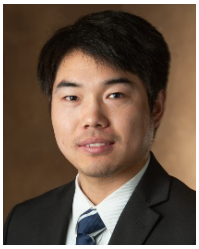

YEYIN XU is currently pursuing the Ph.D. degree with the Harbin Institute of Technology, Harbin, China. His current research interests include nonlinear dynamics, rotor dynamics, and discrete nonlinear systems.

JIAYANG YING received the M.S. degree in mechanical engineering from the Harbin Institute of Technology, Harbin, China, in 2010. His current research interests include fluid dynamics, rotor dynamics, and nonlinear dynamics.